Journal of Alloys and Compounds 509 (2011) 4917–4923

Contents lists available at ScienceDirect

Journal of Alloys and Compounds

journal homepage: www.elsevier.com/locate/jallcom

Room temperature electroresistance in $Sr_{2-x}Gd_xMnTiO_6$ perovskites ($0 \leq x \leq 1$)

N. Biskup [a], M. García-Hernández [a], I. Álvarez-Serrano [b,*], M.L. López [b], M.L. Veiga [b]

[a] Instituto de Ciencia de Materiales de Madrid, Consejo Superior de Investigaciones Cientificas, 28049 Cantoblanco, Madrid, Spain
[b] Departamento de Química Inorgánica I, Facultad de Ciencias Químicas, Universidad Complutense de Madrid, Ciudad Universitaria s/n, E-28040 Madrid, Spain

ARTICLE INFO

Article history:
Received 9 September 2010
Received in revised form 10 January 2011
Accepted 19 January 2011
Available online 26 January 2011

Keywords:
Manganites
Electroresistance
Magnetic
Gadolinium

ABSTRACT

We report on the room temperature strong (~80%) electroresistance (ER) in the double perovskite with mixed Mn valence: $Sr_{2-x}Gd_xMnTiO_6$, $0 \leq x \leq 1$. Both, continuous and pulsed current–voltage curves are almost identical which indicates that the observed electroresistance is not associated with heating. This is also supported by simultaneous temperature measurements. ER is negligible (absent) in the $x = 0$ compound and increases with the increase of Gd content 'x'. The amplitude of ER has a maximum for $x = 0.75$, suggesting that ER is determined by both the double exchange and the Mn^{3+} concentration. At the same time, magnetic interactions change from the antiferromagnetic ($x = 0$) to ferromagnetic ones as $x \to 1$, thus linking the ER with ferromagnetism.

1. Introduction

The electroresistance (ER) has been a highly debated issue in the last decade. The first reference to "electroresistance" dates from the early seventies and it was used to describe a change of electrical resistance in ferromagnetic materials near the Curie point [1]. More recently, after the high-impact report about switching of resistive states in the manganate $Pr_{0.7}Ca_{0.3}MnO_3$ [2], the term ER is used to describe a decrease of resistance in magnetic materials for increasing current [3]. Basically, there are two ways to measure this property: the two-contact method, used in highly insulating thin films [3] and heterostructures, and the four-contact method, used for bulk materials. The most investigated materials have been the mixed valence manganites $RE_{1-x}A_xMnO_3$, RE (rare earth) = La, Pr, ..., A = Ca, Sr, ..., which, being a system with strongly competing structural, magnetic and electronic order, are the best candidate for an ER that is coupled with such kind of order. However, the origin of electroresistance in manganites is strongly disputed. The room temperature non-linear I–V characteristic in thin films has been ascribed to the existence of a depletion layer on the interfaces. On the other hand, several reports of the ER in bulk (both single crystals and polycrystals) manganites conclude that the decrease of resistance is a consequence of Joule heating [4]; the increase of current that passes through an inhomogeneous semiconducting material leads to the Joule heating that can be local and result in the current percolation [5]. Indeed, it is difficult to discern the origin of the ER if one knows that, for example, the magnetic ordering results in the magnetocaloric effect [6]: if the current is able to induce a ferromagnetic order on its path, then the local heating is a logical consequence. The most obvious way to eliminate the heating effect is the application of pulsed measurements. In such a case, the heating should be drastically reduced and the "intrinsic" ER will not be masked by the Joule heating. Such measurements often show no intrinsic ER [7].

We have shown in several manganites that the discontinuous transitions from the high to low resistive state cannot be a consequence of local heating [8]. These discontinuous transitions are seen in pulsed measurements as well. Unfortunately, pulsed measurements are often limited to high temperatures where the resistance of a semiconducting sample is low. In quite a few cases one can confirm the discontinuous resistive transition by pulsed measurements. For $La_{0.9}Sr_{0.1}MnO_3$ we have shown not only that such transitions are present in the low temperature ($T < 150$ K) ferromagnetic state [9], but also that they depend crucially on the internal magnetic and structural order [10].

The situation is quite different in the family of double perovskites where the concept of electroresistance is not used: in some reports considering the electrical conductivity in polycrystalline double perovskites, the observed nonlinear I–V curves are attributed to Joule heating [7] or to grain boundary insulating barrier [11]. These insulating grain boundaries also contribute to the large dielectric constant found in these materials [12]. From the technological point of view, it would be important to confirm the intrinsic, not heat-related ER at the room temperature in order to tailor new materials for applications. It is therefore interesting to

* Corresponding author. Tel.: +34 1 3945237; fax: +34 1 3944352.
E-mail address: ias@quim.ucm.es (I. Álvarez-Serrano).

0925-8388/$ – see front matter © 2011 Elsevier B.V. All rights reserved.
doi:10.1016/j.jallcom.2011.01.130

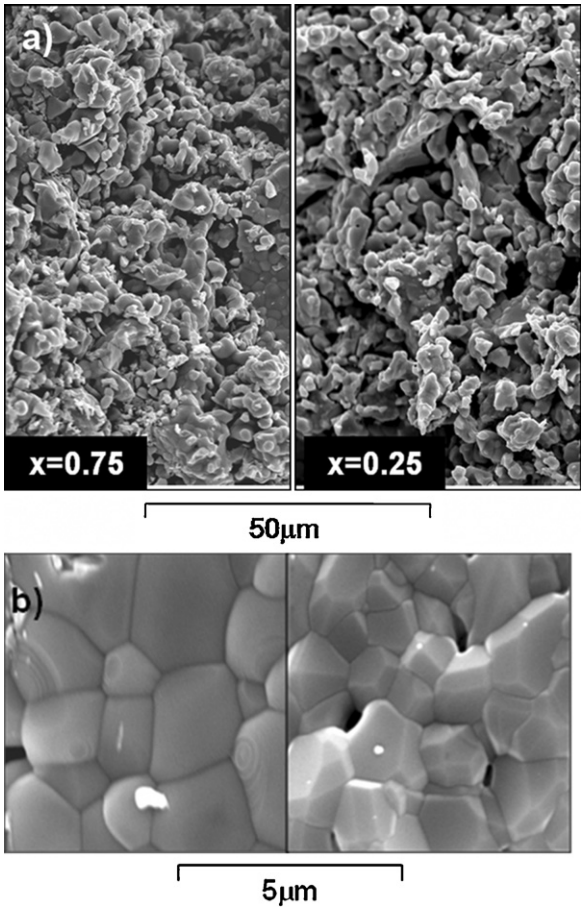

Fig. 1. SEM images of $x = 0.75$ (left) and $x = 0.25$ sample (right).

explore the non-linear I–V characteristic in double perovskites in the light of possible magnetic or structural order. The unit cell of double perovskites $A_2B'B''O_6$ in its simplest form is cubic, containing two corner-sharing, $B'O_3$ and $B''O_3$ octahedra. In the search for novel materials with a high dielectric constant, the double perovskite Sr_2MnTiO_6 was synthesized in 2008 [13,14]. Additional promising properties can be achieved by a partial replacement of strontium with gadolinium: $Sr_{2-x}Gd_xMnTiO_6$ [15]. The introduction of trivalent Gd ion leads to the partial change of manganese valence from Mn^{4+} to Mn^{3+}. Similarly to the case of $RE_{1-x}A_xMnO_3$ manganites, the electron doping (due to introduction of Mn^{3+}) increases the electrical conductivity, in spite of intercalation of Ti ion. We find the small negative magnetoresistance in the whole $Sr_{2-x}Gd_xMnTiO_6$ family, although no long-range double exchange order prevails at any temperature. Further, we report on the room temperature intrinsic electroresistance in a $Sr_{2-x}Gd_xMnTiO_6$ complex perovskite that is identical in both d.c. and pulsed measurements. We discuss this ER in the light of the double-exchange interaction and the structural disorder.

2. Experimental

The details about the synthesis, structural and magnetic characterizations can be found in Ref. [15]. High resolution transmission electron microscopy (HRTEM) and electron diffraction (ED) were performed using a PHILIPS CM200FEG super-twin, with point resolution of 0.24 nm ("C.A.I. Microscopía electrónica U.C.M."). Samples were prepared by crushing the powder under n-butanol and dispersing them over copper grids covered with a holey carbon film. The powder of $Sr_{2-x}Gd_xMnTiO_6$, for all $0 \leq x \leq 1$, was sintered at $T = 1273$ K, with applied pressure of $p = 6$ kbar into the pellets which typical diameter was 5 mm and thickness 1–2 mm. Fig. 1 shows the scanning electron microscopy (SEM) images of two samples: $x = 0.25$ and $x = 0.75$. In the upper panel (50 μm scale) it can be seen that both samples, $x = 0.25$ and $x = 0.75$, are very (indistinguishably) similar from the point of view of porosity and homogeneity. In the lower panel (5 μm scale) it can be seen that the form of grains is different for the two compositions (flat faces and polyhedral facets for $x = 0.25$ and $x = 0.75$, respectively), but that both exhibit similar distributions of melted grain boundaries. Similar results are obtained for all the compositions $0 < x < 1$, and the particular two compositions shown in Fig. 1 ($x = 0.25$ and $x = 0.75$) are chosen because their electrical transport is very different. These images show that the difference in electrical transport properties (resistivity and ER, as will be seen later) between different compositions is not driven by different polycrystalline sintering characteristics.

Magnetic and electrical characterizations are performed in Quantum Design MPMS (squid) and PPMS (Physical Phenomena Measurement System), respectively. Four silver-paint contacts are used in all electrical transport measurements, while two contacts are used in capacitance measurements. Electroresistance measurements are performed in a separate setup consisting of various combinations of current sources and voltmeters. This ensures us that the ER observed is not an artifact due to experimental malfunctioning of a particular instrument. The samples are placed close to a standard platinum thermometer which monitors the temperature increase upon the application of high currents. Additionally, ER was also confirmed in the PPMS system. The I–V curves are symmetric for positive and negative current direction and here we show just 'averaged' resistance values $R = (V(+I) - V(-I))/2I$. In order to minimize the heating effect, pulsed measurements are performed using Keithley models K6221A and K2182A. The pulse lengths are from 0.1 ms to 10 ms, and each successive pulse is delayed by a period of 20 pulse lengths. The choice of the pulse length depends on the resistance of the sample: for larger resistances the pulses had to be larger. Therefore, in the highly resistive samples ($x = 0, 0.75, 1$) the reliable pulsed measurements could not be done at temperatures lower than room temperature. Thus, in order to compare the pulsed and continuous (d.c.) measurements of all samples, here we present just the room temperature measurements. Nevertheless, the observed ER is also confirmed at lower temperatures.

3. Results

The electrical resistivity for $x = 0, 0.25, 0.5, 0.75, 1$ compounds is shown in Fig. 2. Fig. 2a shows the temperature dependence of the resistivity. The incorporation of Gd^{3+} ion, that partially changes the manganese valence $Mn^{4+} \rightarrow Mn^{3+}$, dopes this system with the additional charge carriers leading to a drastic reduction of resistivity of more than two orders of magnitude. The resistivity is lowest for $x = 0.25$ and is increasing again as $x \rightarrow 1$. The $R(T)$ curves do not show any anomaly that would indicate some structural or charge order. $R(T)$ cannot be fitted perfectly either to variable range hopping, or to activated behavior. An example of Arrhenius fit for $x = 0.25$ is shown as a black line in Fig. 2a. In spite of this, in order to show the general tendency, we give both the room temperature resistivities ρ and activation energies Δ (from Arrhenius fits) in Table 1. The rest of the parameters shown in Table 1 are discussed further below.

Both ρ and Δ have minimum values at $x = 0.25$. We have also measured the magnetoresistance $R(B, T = \text{const.})$ and $R(T, B = \text{const.})$ of all samples. Fig. 2b shows the relative decrease of room temperature resistivity for $x = 0$, 0.5 and 1 and the magnitude of MR at $H = 5$ T and $T = 300$ K for all x is given in Table 1. All samples have very small negative magnetoresistance (resistance decreasing in magnetic field) that increases up to 3% at $T = 100$ K, the lowest temperature where the resistance could be measured in four points. Since such changes are indiscernible on the logarithmic scale, we do not plot the $B \neq 0$ resistivity data in Fig. 2a. However, we note that no insulator–metal transition is observed for fields up to $B = 8$ T.

The magnetic characterization of $Sr_{2-x}Gd_xMnTiO_6$ family is shown in Fig. 3. The main panel of Fig. 3a shows the inverse molar susceptibility $1/\chi$, for both zero field cooled (ZFC) and field cooled (FC) measurements. The inset shows the ZFC susceptibility at low temperatures. Two important properties are clearly visible. First, the whole $Sr_{2-x}Gd_xMnTiO_6$ family orders magnetically at $T \approx 43$ K. This is in accordance with the already published results in Sr_2MnTiO_6 [13]. Fig. 3b shows the magnetization in units of Bohr magneton per unit cell for all five compositions at $T = 5$ K. Additionally, for the comparison, we plot the Brillouin function that corresponds to the $x = 1$ compound. The $x = 1$ is a system with $J = 11/2 (J(Gd^{3+}) + J(Mn^{3+}) = 7/2 + 4/2 = 11/2)$. It is clear that experimentally obtained $M(H)$ curve has a larger slope than expected for

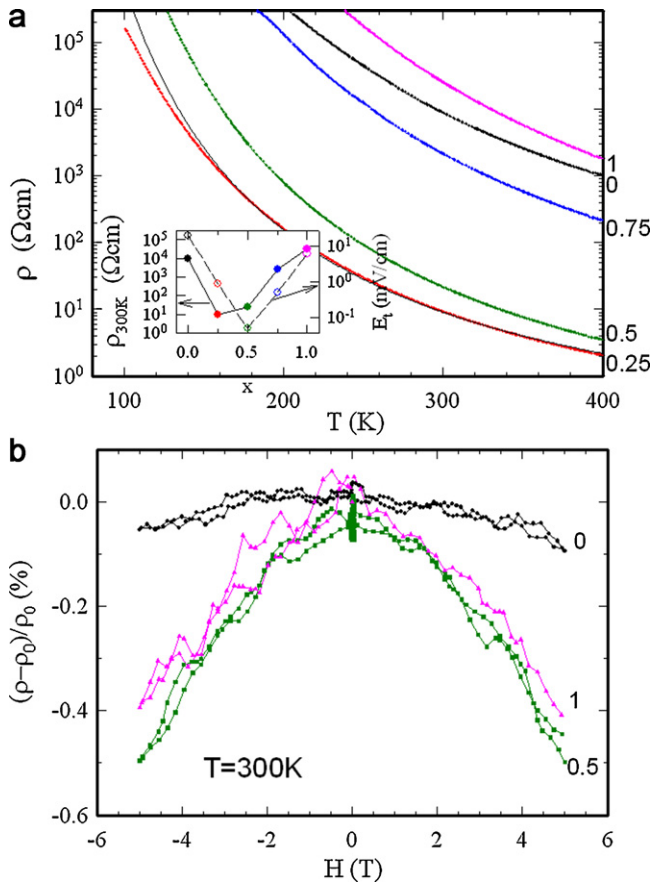

Fig. 2. (a) Resistivity (ρ) vs. temperature (T) for $x = 0$, 0.25, 0.5, 0.75, 1. *Black line:* Arrhenius fit for $x = 0.25$. *Inset:* room temperature resistivity ρ and electrical threshold field E_t as a function of x. (b) Small negative magnetoresistance at $T = 300$ K for $x = 0$, 0.5 and 1. (For interpretation of the references to color in this figure legend, the reader is referred to the web version of this article.)

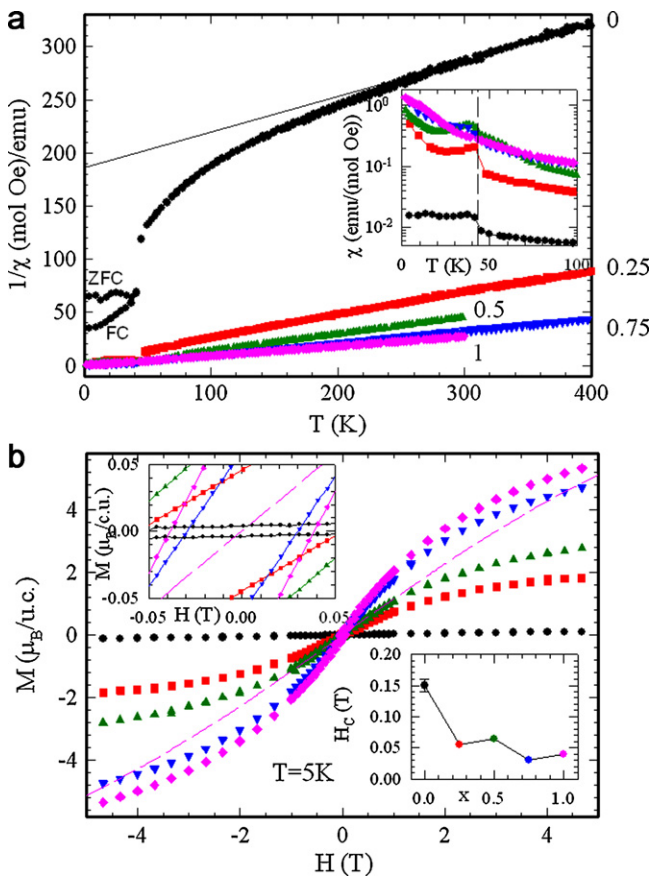

Fig. 3. (a) Inverse molar magnetic susceptibility ($1/\chi$) vs. temperature for $x = 0$, 0.25, 0.5, 0.75, 1 Magnetic field is $H = 500$ Oe. Line is a fit for $x = 0$ in the $250 < T < 400$ K region. *Inset:* low temperature susceptibility vs. temperature. (b) Magnetization in units of Bohr magneton per unit cell as a function of magnetic field H at $T = 5$ K. Broken line is the Brillouin function B_J for $J = 11/2$. *Left inset:* enlarged area around $B = 0$. *Right inset:* coercive field H_C as a function of x.

the case of a paramagnet. In the left inset we plot the enlarged portion of $M(H)$ curve close to zero field. Ferromagnetic (FM) hysteresis exists in all cases. Interestingly, in spite of the smallest magnetic moment, the $x = 0$ compound has the largest coercive field H_C (right inset). We note that this weak ferromagnetism is inherent to the whole family $0 < x < 1$ and does not depend on the electron (Gd^{3+}) doping. The second important property is linked to the high temperature susceptibility. The conventional fit of the inverse molar susceptibility to the Curie–Weiss law $1/\chi(T) = 1/C(T - \theta)$ for the $x = 0$ compound in linear region $250\,\text{K} < T < 400\,\text{K}$ renders a strong antiferromagnetic (AF) interactions with $\theta = -554$ K. The Curie constants C for all compounds $0 \le x \le 1$ are in the limits of theoretically predicted values, but the nature of magnetic interactions changes gradually form AF in $x = 0$ compound to FM for $x \ge 0.5$. From the determination of Curie constant $C = (N_A/3k)\mu_B^2 p^2$ (N_A is the Avogadro number, μ_B is the Bohr magneton and k is the Boltzmann constant) we have extracted the effective number of Bohr electrons 'p' that is listed in Table 1, together with the theoretical value p_{theor} and corresponding Weiss temperatures θ. The AF character of the $x = 0$ compound and its low-temperature FM transition indicate the strong competition between the FM and AF correlations. The $T < 43$ K ferromagnetism is incomplete (frustrated), as indicated by both the differences in ZFC and FC curves and their saturation moments M_S [15].

Fig. 4 summarizes the room temperature ER measurements for five concentrations from top to bottom: $x = 0$, 0.25, 0.5, 0.75, 1. Here we plot the values of resistance instead of resistivity: resistivity values are given in Table 1. The d.c. measurements are plotted as hollow circles. Pulsed measurements of different pulse lengths are shown as full symbols. The colors and shapes of pulsed measurements are given in the figure caption. The current scale is logarithmic in order to cover uniformly the large range of currents. The insets are as following: for the three more resistive samples ($x = 0$, 0.75 and 1), in insets we include the I–V curves. In the case of $x = 0$ and $x = 1$ the negative differential resistance (NDR) $dV/dI < 0$

Table 1
Resistivity ρ, activation energy Δ, magnitude of magnetoresistance at $T = 300$ K and $H = 5$ T, Weiss temperature θ, effective Bohr magneton number p, as calculated and measured, and ER threshold voltage V_T for $0 < x < 1$.

x	ρ (Ω cm)	Δ (eV)	MR (300 K, 5 T) (%)	θ (K)	p_{exp}	p_{calc}	E_t (V/cm)
0	10,000	0.26	−0.10	−554	4.88	4.00	20
0.25	10	0.15	−0.37	−52.8	6.41	5.85	0.9
0.50	25	0.21	−0.44	22.8	6.99	7.24	0.05
0.75	2500	0.32	−0.41	34.6	8.57	8.41	0.5
1	30,000	0.39	−0.41	1.4	9.37	9.43	6

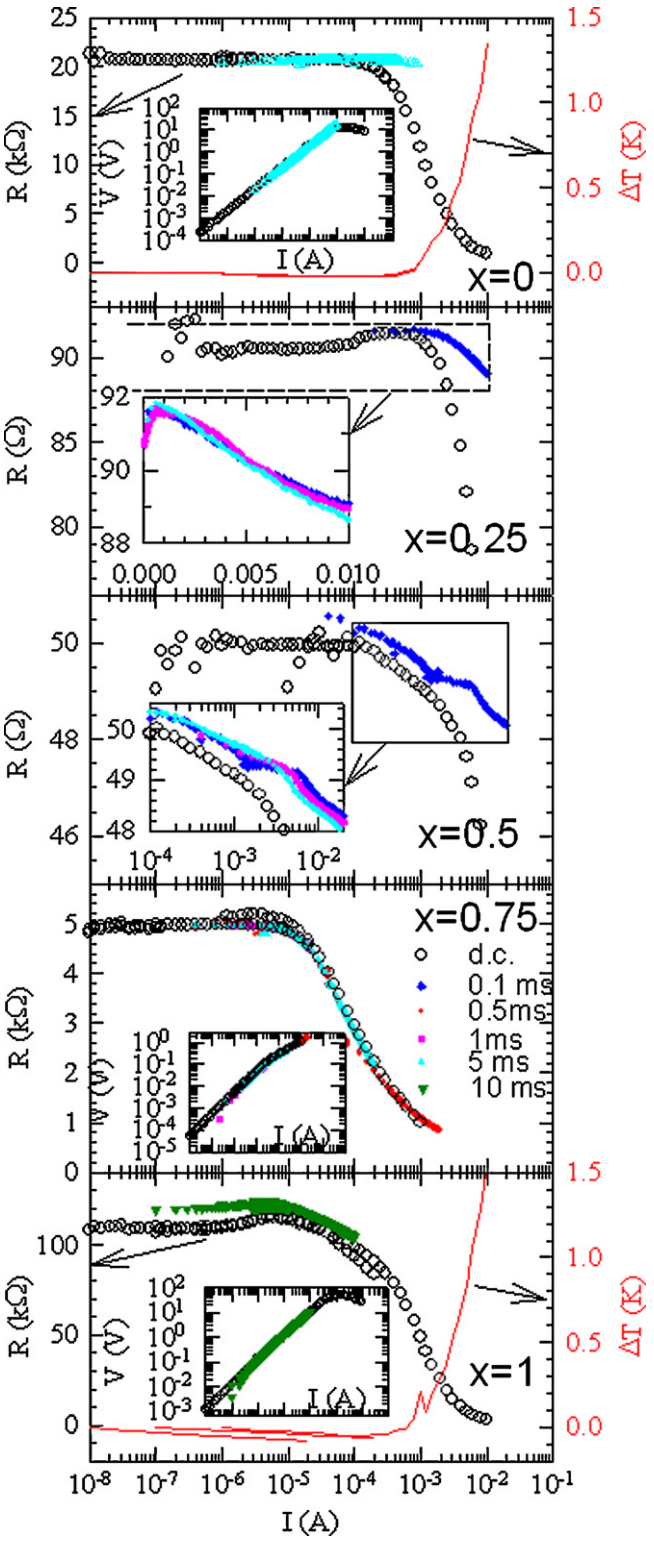

Fig. 4. Resistance vs. current for $x = 0$ (upper panel) to $x = 1$ (lower panel). Black hollow circles denote d.c. measurements. Colored symbols are pulsed measurements, as defined in the figure. Red line in two panels is the temperature increase measured on the thermometer attached to the sample. Inset in $x = 0$, 0.75, 1 panel are I–V curves. Inset in 0.25 and 0.5 panel are enlarged areas as indicated in figure. (For interpretation of the references to color in this figure legend, the reader is referred to the web version of this article.)

is observed at $I > 1$ mA. This NDR is clearly accompanied by heating, as recorded by the on-site thermometer (red line in the main panels). In the case of $x = 0.75$, the I–V curve changes the slope above $I = 10$ μA, but no NDR is observed up to $I = 1$ mA. Note that this "slight" change of $V = f(I)$ curve results in a giant ER when plotted as $R = f(I)$. Consequently, we did not plot I–V curves for $x = 0.25$ and $x = 0.5$ where the change in $R(I)$ is rather small. Instead, for these two cases we have enlarged the portion of $R(I)$ curves in order to appreciate the subtle changes in pulsed measurements. Let us now comment on all of these figures.

For $x = 0$ no intrinsic ER is found, as can be inspected by comparison between the d.c. and pulsed measurements. The huge nonlinearity above $I = 1$ mA is a mere consequence of Joule heating. The red line shows the increase of temperature recorded on a thermometer attached to the sample. The temperature increases rapidly for $I > 1$ mA, although the initial decrease of resistance even below that current is probably also driven by local heating. The temperature increment is quite small ($\Delta T = 1.3$ K) but from the resistance values one can deduce the huge heating in filamentary paths inside the sample. Even the pulsed measurements show some decrease of resistance which is probably also consequence of a small, local heating after the $\Delta t = 5$ ms pulse. Naturally, no bulk increase of temperature can be detected in any pulsed measurements. Finally, it is worth noting that the heating induced ER, as in this example, results in the negative differential resistance (NDR) $dV/dI < 0$.

ER in the case of $x = 0.25$ is slightly different. First, one has to note that the resistance is more than 2 orders of magnitude smaller. This enables us to apply shorter pulses and compare the measurements with different pulse lengths. d.c. measurements show similar huge nonlinearity above $I = 1$ mA that is a consequence of heating. However, much smaller nonlinearity is observed also in the $\Delta t = 0.1$ ms pulse measurements. Therefore, we have limited the resistance range in this panel to $\Delta R = 17\ \Omega$, around the measured $R = 90\ \Omega$. The slight increase of resistance above $I = 0.1$ mA is not uncommon and emphasizes the highly non-Ohmic resistive patterns in these samples. In the inset we show the enlarged area as indicated by broken lines (note that the inset has a linear scale, contrary to the main panel). In this inset we show the three different pulse lengths: 0.1, 0.5 and 1 ms. One can see that at low currents the three curves are identical (inside of experimental error) but that at $I > 6$ mA the resistance obtained by shorter pulse (0.1 ms, blue) decreases less than the one obtained with longer pulse (1 ms, cyan). This indicates that the sample heats up for $I > 6$ mA, at least along the conduction paths. No heating can be observed for lower currents.

The two regimes (ER associated with heating and ER without heating) are even more clearly visible in $x = 0.5$ compound. Here the difference of three pulsed measurements are clearly visible just after the kink at $I = 4$–6 mA. This shows that the intrinsic ER at lower currents (at $I < 4$ mA) probably triggers a heat-releasing process that further enhances the ER.

The $x = 0.75$ compound has the largest ER. The rather well-defined threshold current of 10 μA is observable in both d.c. and pulsed measurements. The most important finding in $x = 0.75$ compound is that ER is identical in both types of measurements. Note that the heating power in $\Delta t = 1$ ms pulse (red squares in Fig. 4) is one thousand times smaller than in the d.c. measurements. This shows that the ER for $x = 0.75$ is not associated to any heating process, at least up to $I = 1$ mA. Finally, in spite of the strong ER (80% at $I = 1$ mA), no NDR is observed, contrary to the heating-induced NDR in $x = 0$.

The $x = 1$ compound is the most resistive and is a good example to neatly observe two different types of ER. Due to the large resistance, we could apply pulsed measurements only with the largest pulse period ($\Delta t = 10$ ms) and in the limited range of currents. But despite these experimental constraints, the comparison of d.c. and

pulsed data enables us to assign the low-current ($I < 200$–$300\ \mu A$) ER as intrinsic, i.e. as the one not associated with heating. For larger currents the temperature starts to increase (red line shows the temperature increase ΔT), and an extra increase is observed above the temperature spike at $I = 1$ mA. Interestingly, the $I = 1$ mA temperature spike also marks the current above which NDR is observed.

Electrical threshold fields are shown in Table 1. Threshold for $x = 0$ is commented by a star, since this ER is different than those for $x > 0$, in the sense that it can only be associated to heating. Nevertheless, the electrical threshold fields for all concentrations show a pronounced minimum at $x = 0.5$ (see Table 1). This indicates that, despite possible local inhomogeneities in each sample, the ER is probably linked to double exchange.

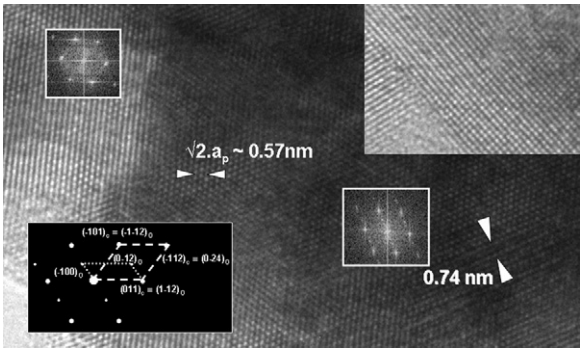

Fig. 5. HRTEM images of $x = 0.75$ compound (a) along $[1\,1\,1]_C$ and (b) $[0\,0\,1]_C$ zone axis; (c) correspondent fast Fourier transforms of (a), and (d) schematic interpretation of FFT. Indexes "c" and "o" refer to cubic and orthorhombic, respectively.

4. Discussion

The electrical transport and magnetic characterizations of the $Sr_{2-x}Gd_xMnTiO_6$ family is generally similar to those of the standard mixed valence manganites [16]. In manganites, when x is close to 0 or 1, an insulating, canted antiferromagnetic ground state is established at low temperatures. In between ($0 < x < 1$), a variety of states can be present, including both FM metallic and FM insulating state. The situation in $Sr_{2-x}Gd_xMnTiO_6$ is similar: the magnetic ground state (low T) for all concentrations $0 < x < 1$ appears to be a canted AF (or frustrated FM) state [15]. The introduction of gadolinium results in a partial change of valence of manganese ions ($Mn^{4+} \rightarrow Mn^{3+}$) and this leads to the drastic reduction of room temperature resistivity. For higher concentrations x, where Mn^{3+} ions dominate, the resistivity starts to increase again. This increase of resistivity is a consequence of charge localization driven by Jahn–Teller distortion of Mn^{3+} ions. Thus, the Ohmic electrical transport in $Sr_{2-x}Gd_xMnTiO_6$ family could easily be explained by the effects of electron (Mn^{3+}) doping and the Jahn–Teller driven charge localization at $x = 0.75$ and $x = 1$. The fact that no metallic conductivity is observed in the temperature behavior of resistance even in fields up to $B = 8$ T indicates that the double exchange is not a dominant factor in the Ohmic electric transport. However, the pronounced minimum in the electrical threshold field E_t at $x = 0.5$, where the double exchange is strongest, suggests that the DE impacts the non-linear electrical transport, As seen in Fig. 4, two types of electroresistance are detected in $Sr_{2-x}Gd_xMnTiO_6$ system. At the highest currents, the ER is accompanied by macroscopic heating (see panels $x = 0$ and $x = 1$). It is difficult to assess the origin of this heating but it appears not to be a bare Joule heating: the comparison of incoming d.c. power $P = I \times V$ for all the values of x shows that the heating starts for different values of P, from 90 μW (case of $x = 0.25$) to 17 mW (case of $x = 1$). When $x = 0$, ER is always accompanied by heating, even in pulsed measurements. On the contrary, for $x > 0$ we are able to distinguish ER with and ER without heating: the second one we call 'adiabatic ER'. We define the ER as adiabatic not only when thermometer shows a stable temperature (since the heating might be local on the current paths in the sample), but also when d.c and pulsed measurements coincide. From Fig. 4 we can see that the magnitude of adiabatic ER increases with the Gd (i.e. Mn^{3+}) content: from no adiabatic ER for $x = 0$ to maximum adiabatic ER ($\Delta R/R_0 = 0.8$ at $I = 1$ mA) for $x = 0.75$. ER then again becomes smaller at $x = 1$. Since no adiabatic ER is found for $x = 0$, this ER at $x > 0$ is clearly a consequence of the change of local magnetic interaction (from AF to FM). We have previously found in $La_{0.9}Sr_{0.1}MnO_3$ that the FM interactions are a prerequisite for a current-induced change from the high resistive state into a low resistive state [9]. In particular, for the case of untwinned single crystal, such a transition is discontinuous, i.e. of the first order while in our polycrystalline samples these microscopic first order transitions are smeared out. What makes the ER in $Sr_{2-x}Gd_xMnTiO_6$ special is the fact that it exists at room temperature, i.e. at temperature well above the temperature of the long-range magnetic order. This indicates that even the short range FM interactions, as shown in Fig. 2, are sufficient requisite for adiabatic ER. Finally, we note that the equivalence of the pulsed and d.c. ER, as shown in the $x = 0.75$ case, has not been seen in either $RE_{1-x}A_xMnO_3$ manganites or in double manganites [7].

Naturally, one has also to consider the current percolation through internal inhomogeneities as the origin of ER in $Sr_{2-x}Gd_xMnTiO_6$. The first source of inhomogeneities is that inherent to double perovskites. Double perovskites are known to exhibit disorder among the cations occupying the B′ and B″ positions [17]. If the valence of two B cations is equal, both cations occupy randomly B′ and B″ sites, an effect known as anti-site-disorder (ASD). This is the case in the parent compound Sr_2MnTiO_6. If the valence of B cations differs by four or more ($A_2B^{2+}B^{6+}O_6$ or $A_2B^{+}B^{7+}O_6$) the B cations are ordered. For the intermediate valence ($A_2B^{3+}B^{5+}O_6$) the tendency of B cation order decreases, yet the complete order is not achieved.

The parent compound Sr_2MnTiO_6 is formed by nanosized cubic crystals with random distribution of ions (Mn or Ti) on the perovskite B-site [14] in spite of showing extended regions of different symmetries coexisting in the same crystals. Both Mn and Ti ions have the same valence (4+) yielding a complete ASD that permits Mn-rich and Ti-rich clusters. In such a system we do not observe the adiabatic ER. The situation changes with doping of Gd^{3+} (and corresponding valence change of Mn^{4+} to Mn^{3+}). Gd^{3+} doping does not introduce order in the B sublattice, as confirmed by structural measurements, and the system still contains Mn-rich clusters. But part of the manganese ions is now Mn^{3+} which promotes the double exchange interaction in these clusters. This effect might be responsible for the pronounced minima of threshold electrical field E_t at $x = 0.5$ when the largest numbers of Mn^{3+}–O–Mn^{4+} links are established. We also note that the negative magnetoresistance (Fig. 2b) is largest at $x = 0.5$.

The second source of inhomogeneities inside the manganese rich clusters could be associated with both structural and microstructural disorder (i.e. random distribution at B sites and extended defects, multitwinning, etc., respectively). Fig. 5 shows HRTEM images of the $x = 0.75$ compound. One can observe the existence of orthorhombic (pseudotetragonal) regions with different orientations on the nanometer scale. The structural analysis shows that the crystal structure gradually changes from cubic to orthorhombic as $x \rightarrow 1$ [15]. This is in accordance with the increased number of Mn^{3+} ions that suffer Jahn–Teller distortion. It is well known from $RE_{1-x}A_xMnO_3$ manganates that Jahn–Teller distortion competes with DE interaction. Thus, as $x \rightarrow 1$, the resistivity also increases due to suppression of DE by Jahn–Teller distortion. In the case of existence of different domains, as those shown in Fig. 5, the

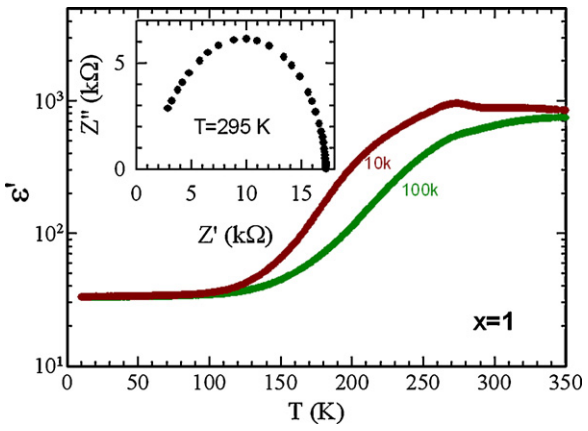

Fig. 6. Temperature dependence of dielectric constant ε' in $SrGdMnTiO_6$ for $f = 10$ kHz and $f = 100$ kHz. *Inset:* complex impedance plot Z''–Z' at $T = 300$ K.

current percolation through a mixed Mn^{3+}–Mn^{4+} regions where no Jahn–Teller order is established, might be behind the giant adiabatic ER observed for $x = 0.75$. However, adiabatic ER is found also for $x = 1$. In this case, all the manganese ions are Mn^{3+} and the whole material has orthorhombic structure. We have shown that the "large" electrical current can suppress the orbital order in $La_{0.9}Sr_{0.1}MnO_3$, resulting in colossal ER at low temperatures [9]. In $Sr_{2-x}Gd_xMnTiO_6$ ceramic no orbital or charge order is seen either in temperature behavior of resistivity (this one explored up to 1273 K) or in magnetization. This, however, does not exclude the influence of large currents/voltages on orbital configurations and/or Jahn–Teller distortion in $x > 0$ compounds. The electron hopping (current) induced suppression of Jahn–Teller distortion should be local, on the local current paths. This type of percolation effect might explain the subtle differences in resistance close to the threshold voltage V_T, for example, the initial increase of R for $x = 0.25$ or $x = 1$.

Finally, one source of inhomogeneities in polycrystalline samples is, naturally, the grain boundaries. A future synthesis of single crystals will definitely eliminate the grain borders as the origin of ER in $Sr_{2-x}Gd_xMnTiO_6$. However, even in polycrystalline samples we have seen enough indication that magnetic interactions and double exchange play a dominant role in ER. We have seen in Fig. 1 that we have good ceramics with similar distributions of melted grain boundaries. Fig. 6 shows the temperature dependence of dielectric constant of the $SrGdMnTiO_6$ ($x = 1$) sample for two frequencies: $f = 10$ kHz and $f = 100$ kHz. The high value of dielectric constant ε at room temperature decreases with lowering temperature to $\varepsilon \approx 30$ at $T < 100$ K. $\varepsilon \approx 30$ is a typical value of dielectric constant of a perovskite crystalline structure [18] and the giant, room temperature value ($\varepsilon \approx 1000$) is a consequence of electrical inhomogeneities of this material. Similar $\varepsilon(T)$ curves are found in all compositions $0 < x < 1$. This type of $\varepsilon(T)$ curves is typical for polycrystalline samples: at high temperatures where the intrinsic, intragrain resistivity is smaller than intergrain (grain boundaries) resistivity, electric charge is accumulated on the grain boundaries and the capacitance of such a system is high. By lowering the temperature, the intragrain resistivity eventually (if the intragrain activation energy is larger than intergrain activation energy) overcomes the resistance of grain boundaries resulting in a decrease of the accumulated charge and, consequently, in a decrease of dielectric constant. In inset of Fig. 6 we show the complex impedance plot Z'' vs. Z' (Cole–Cole plot) taken at $T = 300$ K, the temperature of our ER study. The single semicircle of such a plot indicates that our system can be modeled by a single R–C element defined by the grain boundaries and resulting in $\varepsilon \approx 1000$. Thus, we are aware that the electrical transport is influenced, if not dominated, by grain boundaries. However, it is not straightforward to imagine that the ER changes with doping 'x' only due to changes in grain boundaries. We have seen in Fig. 1 that the grain size distributions in the polycrystals is the same for all $0 < x < 1$, while the ER changes drastically. So, even if the ER arises through some processes associated to grain boundaries, these processes are intrinsic and characteristic of particular composition. The above-mentioned ASD, Jahn–Teller distortion or orbital order is present even at the grain boundaries.

5. Conclusions

We report on the room temperature electroresistance in $Sr_{2-x}Gd_xMnTiO_6$. Apart of the usual, heating-associated ER, we find an 'adiabatic' ER, i.e. one that is identical in pulsed and d.c. measurements. We interpret the ER accompanied by heating as a consequence of Joule heating, at least in $x = 0$ compound. Adiabatic ER, on the other side, is interpreted as the current induced suppression of Mn^{3+} orbital order and/or Jahn–Teller distortion. The electrical threshold field for adiabatic ER is lowest at $x = 0.5$, suggesting that the double exchange might be responsible for the nonlinear conductivity. The magnetic interactions at room temperature shift from AF toward FM (see parameter θ in Table 1), coinciding with the appearance of adiabatic ER. The ER threshold field E_t depends on the concentration x similarly to the magnitude of MR (Fig. 2b and Table 1), underlying the link between the magnetism and ER. Structural/magnetic inhomogeneities in compounds with $x > 0$ might also play a role in a current percolation. Thus, we do not discard the possibility that the heating-associated ER in $x > 0$ compounds originates from the local magnetic reordering. Particularly, the complex structure of this double perovskite (intercalation of Ti ion between adjacent manganese ions) might be responsible for the observance of 'adiabatic' ER: the long range magnetic (ferro) ordering is impeded by magnetically inert Ti ions. This might explain why in simple mixed-valence manganites $L_{1-x}A_xMnO_3$ (L = La, Pr, Nd, ..., A = Sr, Ca, ...), where the long range magnetic order is not impeded by non-magnetic ions, the ER is always accompanied by heating. Naturally, a thorough structural and magnetic study together with ER measurements in single crystals should give a definite confirmation of this picture.

Acknowledgments

We acknowledge financial support from Spanish Ministerio de Ciencia e Innovación – MAT2003-01880, MAT2010-20117, MAT-2005-06024-C02-01, MAT-2008-06517-C02-01, CSD2009-00013 and also from Comunidad de Madrid – 07N/0080/2002. Authors are grateful to the CAI centers of UCM (XRD and Electron Microscopy).

References

[1] V.N. Kashcheev, Phys. Lett. 31A (1970) 140.
[2] A. Asamitsu, Y. Tomioka, H. Kuwahara, Y. Tokura, Nature (London) 388 (1997) 50.
[3] A. Odagawa, H. Sato, I.H. Inoue, H. Akoh, M. Kawasaki, Y. Tokura, T. Kanno, H. Adachi, Phys. Rev. B 70 (2004) 224403.
[4] S. Mercone, R. Frésard, V. Caignaert, C. Martin, D. Saurel, C. Simona, G. André, P. Monod, F. Fauth, J. Appl. Phys. 98 (2005) 023911;
J. Sacanell, A.G. Leyva, P. Levy, J. Appl. Phys. 98 (2005) 113708;
Y.F. Chen, M. Ziese, P. Esquinazi, Appl. Phys. Lett. 89 (2006) 082501.
[5] M. Tokunaga, Y. Tokunaga, T. Tamegai, Phys. Rev. Lett. 93 (2004) 037203.
[6] X.X. Zhang, J. Tejada, Y. Xin, G.F. Sun, K.W. Wong, X. Bohigas, Appl. Phys. Lett. 69 (1996) 3596.
[7] B. Fisher, J. Genossar, K.B. Chashka, L. Patlagan, G.M. Reisner, Appl. Phys. Lett. 88 (2006) 152103.
[8] N. Biškup, A. de Andrés, Phys. Rev. B 74 (2006) 184403.
[9] N. Biškup, A. de Andrés, N.M. Nemes, M. García-Hernandez, K.V. Glazyrin, Y.M. Mukovskii, Appl. Phys. Lett. 90 (2007) 222502.
[10] A. de Andrés, N. Biškup, M. García-Hernández, Y.M. Mukovskii, Phys. Rev. B 79 (2009) 014437.

[11] D. Niebieskikwiat, A. Caneiro, R.D. Sánchez, J. Fontcuberta, Phys. Rev. B 64 (2001) 180406.
[12] K.R.S. Preethi Meher, K.B.R. Varma, J. Appl. Phys. 105 (2009) 034113.
[13] J. Roa-Rojas, C. Salazar, D. Llamos P., A.A. Leon-Vanegas, D.A. Landinez Tellez, P. Pureur, F.T. Dias, V.N. Vieira, J. Magn. Magn. Mater. 320 (2008) E104.
[14] I. Álvarez-Serrano, M.A. Arillo, M. García-Hernández, M.L. López, C. Pico, M.L. Veiga, J. Am. Ceram. Soc. 93 (8) (2010) 2311–2319.
[15] I. Álvarez-Serrano, M.L. López, M.A. Arillo, M. García-Hernández, E. Rodríguez-Castellón, A. Jiménez-López, M.L. Veiga, C. Pico, J. Am. Ceram. Soc 94 (1) (2011) 269–276.
[16] E. Dagotto, T. Hotta, A. Moreo, Phys. Rep. 344 (2001) 1.
[17] F. Galasso, Structure Properties and Preparation of Perovskite-Type Compounds, Pergamon Press, Oxford, 1969.
[18] L. He, J.B. Neaton, M.H. Cohen, D. Vanderbilt, Phys. Rev. B 65 (2002) 214112; D. Capsoni, M. Bini, V. Massarotti, G. Chiodelli, M.C. Mozzatic, C.B. Azzoni, J. Solid State Chem. 177 (2004) 4494.